Rapid chemotactic response enables marine bacteria to exploit ephemeral microscale nutrient patches

Roman Stocker*†, Justin R. Seymour*, Azadeh Samadani‡, Dana E. Hunt*, and Martin F. Polz*

*Department of Civil and Environmental Engineering, Massachusetts Institute of Technology, 77 Massachusetts Avenue, Cambridge, MA 02139; and ‡Department of Physics, Brandeis University, 415 South Street, Waltham, MA 02454

Edited by David M. Karl, University of Hawaii, Honolulu, HI, and approved January 22, 2008 (received for review October 14, 2007)

Because ocean water is typically resource-poor, bacteria may gain significant growth advantages if they can exploit the ephemeral nutrient patches originating from numerous, small sources. Although this interaction has been proposed to enhance biogeochemical transformation rates in the ocean, it remains questionable whether bacteria are able to efficiently use patches before physical mechanisms dissipate them. Here we show that the rapid chemotactic response of the marine bacterium *Pseudoalteromonas haloplanktis* substantially enhances its ability to exploit nutrient patches before they dissipate. We investigated two types of patches important in the ocean: nutrient pulses and nutrient plumes, generated for example from lysed algae and sinking organic particles, respectively. We used microfluidic devices to create patches with environmentally realistic dimensions and dynamics. The accumulation of *P. haloplanktis* in response to a nutrient pulse led to formation of bacterial hot spots within tens of seconds, resulting in a 10-fold higher nutrient exposure for the fastest 20% of the population compared with nonmotile cells. Moreover, the chemotactic response of *P. haloplanktis* was >10 times faster than the classic chemotaxis model *Escherichia coli*, leading to twice the nutrient exposure. We demonstrate that such rapid response allows *P. haloplanktis* to colonize nutrient plumes for realistic particle sinking speeds, with up to a 4-fold nutrient exposure compared with nonmotile cells. These results suggest that chemotactic swimming strategies of marine bacteria in patchy nutrient seascapes exert strong influence on carbon turnover rates by triggering the formation of microscale hot spots of bacterial productivity.

chemotaxis | marine snow | microfluidics | patchiness

Marine bacteria inhabit a complex environment where nutrients are typically concentrated in small (micrometers to centimeters), often ephemeral, patches (1–4), which can contain biologically labile organic compounds at concentrations two to three orders of magnitude above ambient seawater (2, 5, 6). Sources of transient patches include phytoplankton photosynthetic products (4, 7), zooplankton excretion (8), cell lysate (2), and organic matter leaking from particles (6). Although individual patches of dissolved organic matter (DOM) are small, they are abundant; hence the efficiency of marine bacteria in using nutrient patches exerts a fundamental control on biogeochemical transformation rates in the ocean (1, 9). However, it has never been quantitatively evaluated whether the chemotactic response of marine bacteria is rapid enough to enable significant gain from nutrient patches in the face of their rapid physical dissipation.

Motile bacteria can secure a significant advantage from a transient nutrient source only if the biological time scale (τ_{BIO}) of their response is shorter than the time scale (τ_{PHYS}) over which physical processes homogenize the patch, i.e., if $\tau_{BIO} < \tau_{PHYS}$. For stationary nutrient pulses generated by a lysing cell or a sloppy feeding event, τ_{PHYS} is set by diffusion, whereas for moving sources such as a sinking particle, τ_{PHYS} is further influenced by advection (10). Attraction to microscale nutrient patches in the environment has been inferred from observations of bacterial clusters around sporadic protist lysis events (2) and nutrient-loaded beads (11). The potential quantitative importance of these microscale interactions has emerged from theoretical models (5–7), yet the study of environmentally realistic patch-evolution scenarios has been hampered by technical limitations in the laboratory and by the small scale and intermittency of patch dynamics *in situ* (12).

Here, we ask to what extent marine bacteria are capable of exploiting ephemeral nutrient patches generated at environmentally realistic spatiotemporal scales. We use microfluidic devices to generate two types of patches that are expected to occur widely in the ocean (9): a purely diffusive pulse and a plume governed by diffusion and advection. Microfluidic techniques have previously been used to gain insight into different aspects of microbial ecology, including chemotaxis (13) and population behavior within complex landscapes (14, 15). Here, we have fabricated microchannels that create patches with spatial and temporal scales consistent with those expected in the ocean. By simultaneously measuring the spatiotemporal distribution of nutrients and cells, we quantified the nutrient exposure experienced by chemotactic marine bacteria.

Results

Diffusing Nutrient Pulse. We examined the chemotactic response to a diffusing nutrient patch of the marine γ-proteobacterium *Pseudoalteromonas haloplanktis*, which has previously served as a model of chemotaxis (11). We simulated a nutrient pulse by using a microinjector (Fig. 1*a*), which generated a one-dimensional (1D), 300-μm wide band of nutrients (Fig. 1*b*), mimicking the sudden release of organic matter associated with viral lysis or sloppy predation of phytoplankton cells (2). The chemoattractant consisted of culture filtrates from the marine phytoplankton *Dunaliella tertiolecta*. Although patch composition in the ocean is poorly characterized, phytoplankton-derived DOM was chosen because it is likely a significant nutrient component of many patches (4, 5, 16, 17). Algal-derived dissolved organic carbon (DOC) concentration in the culture filtrates (567 μM) was on the high end of measured bulk DOC concentrations during phytoplankton blooms (e.g., ref. 18), representative of conditions in a patch. We use the response to model chemoattractants as indicative of the response to nutrients and hereafter employ the words "nutrient" and "chemoattractant" interchangeably. In the microfluidic channel, bacteria were advected along both sides of the nutrient band. The experiment was initiated by turning off the flow ($t = 0$), causing fluid motion to stop instantaneously and nutrients to diffuse laterally. Thereafter, we recorded the across-channel (x direc-

Author contributions: R.S., J.R.S., and M.F.P. designed research; R.S., J.R.S., and A.S. performed research; R.S. analyzed data; and R.S., J.R.S., D.E.H., and M.F.P. wrote the paper.

The authors declare no conflict of interest.

This article is a PNAS Direct Submission.

†To whom correspondence should be addressed. E-mail: romans@mit.edu.

This article contains supporting information online at www.pnas.org/cgi/content/full/0709765105/DC1.

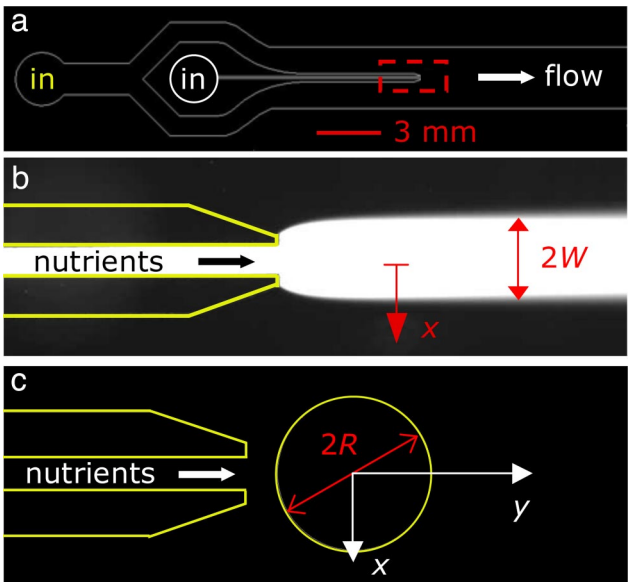

Fig. 1. Microchannels used to probe the chemotactic response of bacteria to nutrient patches and plumes. (*a*) Microchannel for diffusing nutrient pulse experiments. The two inlets (''in'') are for bacteria (yellow) and chemoattractant (white). (*b*) Microinjector tip, corresponding to the red dashed box in *a*. The 300-μm-wide injected nutrient band was visualized by using 100 μM fluorescein. (c) Cylindrical particle (R = 250 μm) used in the nutrient plume experiments.

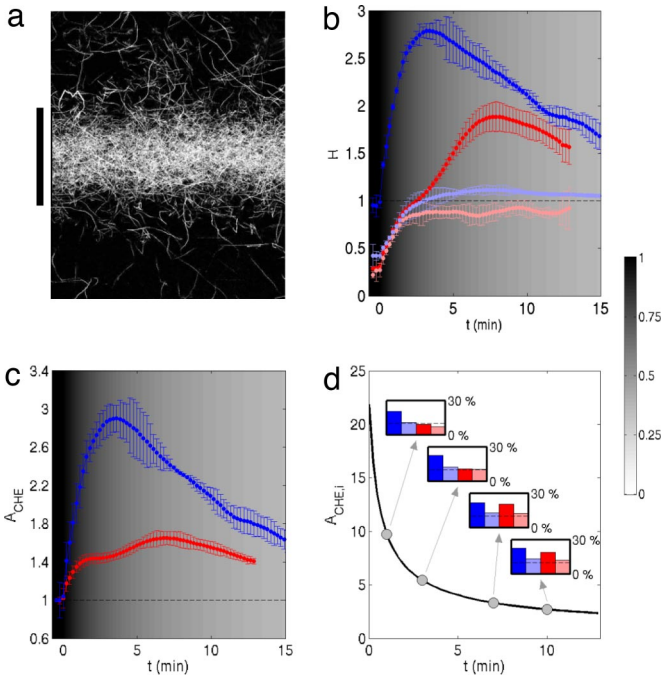

Fig. 2. Response to a nutrient pulse. (*a*) Trajectories of *P. haloplanktis*, 2 min after release of a 300-μm-wide nutrient pulse (black bar). Each white path is an individual trajectory. (*b*) Time evolution of the hot spot index H for *P. haloplanktis* (blue, with chemoattractant; light blue, control run) and *E. coli* (red, with chemoattractant; light red, control run). Initially $H < 1$ because the nutrient band is devoid of bacteria. (*c*) Mean chemotactic advantage index A_{CHE} over nonmotile cells. The gray background and associated color bar indicate the mean nutrient concentration within the central 300-μm region, normalized by its initial value. Color scheme as in *b*. (*d*) Chemotactic advantage $A_{CHE,i}$ of individual bacteria inside the central 300-μm region relative to those outside. (*Insets*) The fraction of the population inside the central band at four points in time (the color scheme is as in *b*).

tion) distribution of both nutrients $C(x)$ and bacteria $B(x)$ every 13 s for at least 13 min. The nutrient distribution was visualized by using fluorescein, which has a diffusivity ($D = 0.5 \times 10^{-9}$ m^2 s^{-1}) typical of low molecular weight substances. Measurements of $C(x)$ showed that the patch diffused from an original width of 300 μm to $\approx$1 mm within 3 min, at which time only 40% of the original nutrients remained within the central 300 μm.

Because the nutrients diffused outwards, *P. haloplanktis* cells strongly aggregated at the center of the band (Fig. 2*a*) within tens of seconds, forming a hot spot, which persisted for at least 15 min. To quantify the magnitude and time scale of the accumulation, we define a hot spot index H as the mean concentration of bacteria within the central 300-μm region relative to the mean concentration over the entire channel width. We expect two components of bacterial motility to determine H: random motility (19), which tends to make the bacterial distribution uniform ($H = 1$), and chemotaxis, which induces aggregation in the patch ($H > 1$). The rapid and strong chemotactic response of *P. haloplanktis* is reflected by a maximum accumulation H_{MAX} = 2.8 within 2.9 min. A 50% increase in concentration over uniform (H = 1.5) was reached within 0.5 min. After reaching a maximum, H decayed as the nutrient gradient subsided, and random motility became progressively more important compared with chemotactic aggregation.

To compare the performance of *P. haloplanktis* with the classic model of bacterial chemotaxis (19), we repeated the experiments with *Escherichia coli*, which was exposed to a nutrient band composed of a mixture of two of its most potent chemoattractants at near-optimal concentrations (serine and aspartate, 10 μM each; H. Berg and L. Turner, personal communication). The chemotactic response of *E. coli* was markedly slower and the accumulation was less intense, taking 7.0 min to reach H_{MAX} = 1.9 and 5.0 min to reach H = 1.5. To focus on the role of chemotaxis without random motility effects, we calculated an accumulation-doubling time scale $\tau_D = (1/H \cdot dH/dt)^{-1}$ at $H = 1$. Comparison revealed that *P. haloplanktis* (τ_D = 0.6 min) was more than 10 times faster (smaller τ_{BIO}) at chemotaxing into the nutrient patch than *E. coli* (τ_D = 7.5 min). This partly reflects a difference in mean swimming speed V_B (68 μm s^{-1} for *P. haloplanktis*; 31 μm s^{-1} for *E. coli*). A quick response is critical because the mean nutrient concentration inside the central region decays rapidly, as shown by the background gray shading in Fig. 2*b*; between 0.5 and 5.0 min, it decreased by 55%.

Motility significantly enhanced the nutrient exposure of a population of *P. haloplanktis*, measured by integrating the nutrient exposure experienced by each cell, or $\int B(x)C(x)dx$. The instantaneous chemotactic advantage relative to a theoretical population of nonmotile cells (taken as the initial distribution $B_I(x)$ of the motile cells) can then be computed as $A_{CHE} = \int B(x)C(x)dx / \int B_I(x)C(x)dx$ and was almost 3 for *P. haloplanktis* (Fig. 2*c*). A_{CHE} applies to bacteria not initially present in the patch because the latter is initially devoid of cells. The significantly faster chemotactic response allowed *P. haloplanktis* to achieve an 87% greater advantage than *E. coli* when averaged over the first 5 min and 64% greater over the first 10 min. These A_{CHE} values represent averages over the entire population, but the first cells entering the patch can do significantly better. Fig. 2*d* shows the advantage $A_{CHE,i}$ experienced by the bacteria that clustered within the central 300-μm region versus those outside. At t = 1 min, 20% of the *P. haloplanktis* population had accumulated in the band and experienced a 10-fold advantage (Fig. 2*d Inset*), whereas *E. coli* and the controls showed insignificant accumulation above background.

To determine how the 1D case investigated here relates to a three-dimensional (3D) scenario in the ocean, we numerically simulated the chemotactic advantage experienced by 10,000

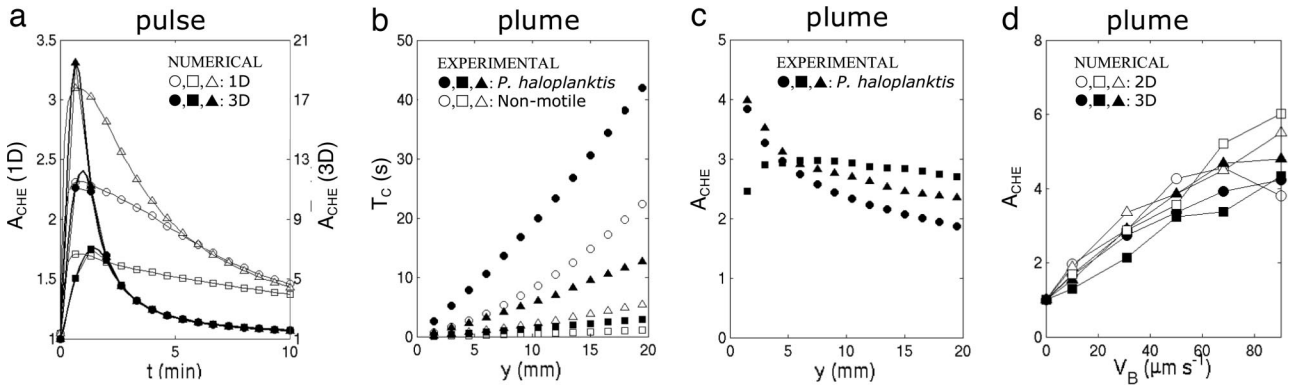

Fig. 3. Experimental and numerical bacterial response. (*a*) Chemotactic advantage A_{CHE} from numerical simulations of chemotactic bacteria exposed to a 1D (open symbols) and a 3D (closed symbols) nutrient pulse, for three swimming speeds (circles, V_B = 31 μm s^{-1}; squares, V_B = 68 μm s^{-1}; and triangles, V_B = 150 μm s^{-1}). The 3D pulse was modeled as the lysis of a 30-μm radius algal cell. (*b*) The equivalent exposure time T_C from a nutrient plume for *P. haloplanktis* and a nonmotile population, determined experimentally for three particle sinking speeds (circles, U = 66 μm s^{-1}; squares, U = 220 μm s^{-1}; triangles, U = 660 μm s^{-1}). (*c*) Experimental A_{CHE} of *P. haloplanktis* as a function of position y in the plume, for the same U as in *b*. (*d*) Numerical A_{CHE} in the plume of a cylinder (2D) and a sphere (3D) as a function of swimming speed V_B, for the same U as in *b*.

chemotactic bacteria responding to a 1D nutrient band and a 3D spherical patch [Fig. 3*a* and supporting information (SI) *Appendix 1*, "Numerical Model"]. The time evolution of A_{CHE} in 1D was comparable with our measurements (Fig. 3*a*). On the other hand, A_{CHE} was approximately five times larger in the 3D scenario for swimming speeds between 31 and 150 μm s^{-1} and patches larger than 10 μm, suggesting that the microchannels provide conservative estimates of chemotactic advantage in the ocean.

Nutrient Plumes. Microscale sources of DOM in the ocean are often in motion relative to their ambient environment, and advection can stretch released solutes into elongated plumes. Nutrient-enriched plumes are predicted to arise from rapid dissolution of fresh fecal pellets (20) and in the wake of marine snow particles (6), where DOM is released because of polymer hydrolysis by particle-attached bacteria (21). Nutrient plumes could represent an important resource for chemotactic bacteria, provided they respond rapidly. We investigated the response of *P. haloplanktis* to a nutrient plume composed of culture filtrates from *D. tertiolecta* by using the microchannel in Fig. 1*a* with a microfabricated polydimethylsiloxane (PDMS) cylinder in front of the injector to model a particle (Fig. 1*c*). Because *P. haloplanktis* is superior in using patchy resources, we focus here on the effect of particle sinking speed, rather than a comparison with *E. coli*. To simulate sinking at speed U, the particle was stationary and immersed in a steady flow of mean velocity U, varied from 66 to 660 μm s^{-1} (5.7–57 m day^{-1}), consistent with empirically predicted values in the ocean [U = 50–500 μm s^{-1} for particles of radius R = 250 μm (22, 23)]. To mimic DOM leakage from the particle, nutrients were added immediately upstream via the microinjector and advected around the particle by the flow, forming a plume in its wake (Fig. 4*a*). The shape of the plume is dictated by the Peclet number Pe = $2UR/D$, a larger Pe corresponding to more slender plumes. Here D is the diffusivity of chemoattractants, assumed to be 0.5×10^{-9} m^2 s^{-1}, a value typical of low molecular weight substances. The radius of the particle (R = 250 μm) is consistent with the size of a small marine snow aggregate or a large fecal pellet (17, 22).

Bacteria introduced upstream (Fig. 1*a*) were advected past the particle and exposed to the nutrient plume. For moderate sinking speeds, *P. haloplanktis* cells aggregated rapidly in the plume (e.g., Fig. 4*a*, U = 110 μm s^{-1}). The accumulation was quantified (Fig. 4 *b2*, *c2*, and *d2*) for three sinking speeds U (66, 220, and 660 μm s^{-1}), corresponding to increasing Pe (66, 220, and 660) and thus narrower plumes (Fig. 4 *b1*, *c1*, and *d1*). We confined our measurements to the first 24 mm of the plume (y = 96 R), where the highest chemoattractant concentrations occur and the disruptive effects of turbulence will be smallest in the ocean (24).

For the slowest sinking speed (U = 66 μm s^{-1}), comparable with the bacterial swimming speed (V_B = 68 μm s^{-1}), the entire "history" of plume detection and exploitation was captured. Accumulation occurred immediately behind the particle and increased downstream, generating an intense hot spot of bacteria with a maximum at y = 4–8 mm, where the concentration of bacteria inside the plume was 4-fold higher than outside. At this position, the time available for bacteria to respond had been $\tau_{PHYS} \approx y/U$ = 2 min (Fig. 4*b2*). Further downstream, as nutrients diffused laterally, the bacterial hot spot gradually relaxed toward a nearly uniform distribution at y = 24 mm ($\tau_{PHYS} \approx$ 6 min). *P. haloplanktis* also accumulated in the plume of a particle sinking at U = 220 μm s^{-1} (Fig. 4*c2*); although plume colonization did not begin immediately behind the particle, it occurred within y = 2 mm (τ_{PHYS} < 10 s). Thereafter, accumulation intensified and broadened, although to a smaller extent than at U = 66 μm s^{-1}, with a less clearly defined peak at $y \approx$ 12 mm. For the fastest particle (U = 660 μm s^{-1}) (Fig. 4*d2*), bacteria swam into the plume but did not form a hot spot, although τ_{PHYS} = 36 s at y = 24 mm. This aspect will be discussed after introducing a measure of nutrient exposure.

By using the measured bacteria and nutrient distributions, we computed the time integral of the nutrient concentration experienced by an average cell in its journey through the plume. Normalizing this by the nutrient concentration at the particle surface, as done in Ref. 10, yielded a measure of nutrient exposure, T_C, as the equivalent time spent by each bacterium in the region adjacent to the particle. T_C increased nearly linearly with downstream position for all sinking speeds (Fig. 3*b*). In the first 20 mm of the plume, U = 66, 220, and 660 μm s^{-1} (τ_{PHYS} = 303, 91, and 30 s) resulted in T_C = 42, 13, and 2.5 s, respectively. By also computing T_C for a population of nonmotile cells, we determined the mean chemotactic advantage A_{CHE} as a function of position in the plume. Although outward diffusion of the plume exposed even nonmotile cells to nutrients (Fig. 3*b*), A_{CHE} was always >1 (Fig. 3*c*), showing that chemotaxis considerably enhanced nutrient exposure in all cases. For the fastest particle, A_{CHE} increased at first as some bacteria swam into the plume, decreasing thereafter as the plume broadened (Fig. 3*c*). For the

ENVIRONMENTAL SCIENCES

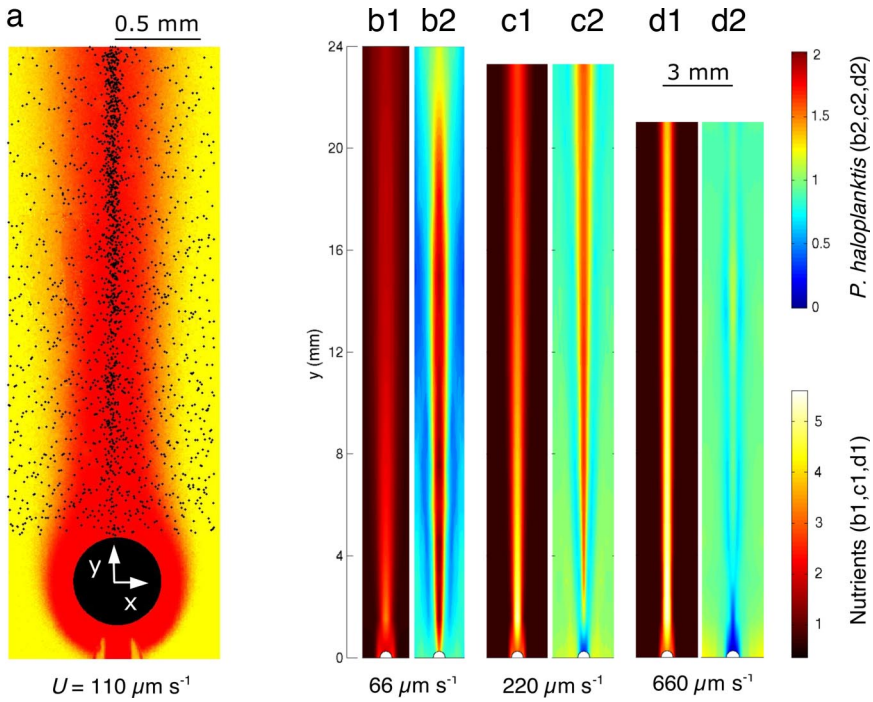

Fig. 4. Response to a nutrient plume. (*a*) Accumulation of *P. haloplanktis* in the nutrient plume of a particle sinking at $U = 110\ \mu m\ s^{-1}$. Flow is from bottom to top, and each black dot represents one bacterium. Red indicates higher nutrient concentration. (*b–d*) Distribution of nutrients (*b1*, *c1*, and *d1*) and *P. haloplanktis* (*b2*, *c2*, and *d2*) normalized to a mean of 1, for three sinking speeds (*U*). The distribution of *P. haloplanktis* was found by binning positions of individual bacteria from a grid of 17 (in *y*) by 3 (in *x*) images. Control runs are shown in *SI Appendix 1* Fig. 5.

slowest particle, fast-responding bacteria obtained a 4-fold chemotactic advantage over nonmotile cells.

T_C decreases with U for a given plume length (Fig. 3*b*), as expected because of reduced time τ_{PHYS} spent in the plume as U increases. However, the absence of significant accumulation at $U = 660\ \mu m\ s^{-1}$ (Fig. 4*d2*) despite $\tau_{PHYS} = 36$ s suggests that A_{CHE} is not only a function of τ_{PHYS}. To test whether A_{CHE} is in fact independent of U for a given τ_{PHYS}, we compared A_{CHE} for the three sinking speeds at the same τ_{PHYS} (30 s). A_{CHE} decreased from 3.7 to 2.7 for U increasing from 66 to 660 $\mu m\ s^{-1}$, indicating that A_{CHE} depends on the specific plume dynamics set by the Peclet number and not purely on τ_{PHYS} [possibly a result of bacteria taking a disproportionate advantage of the low-velocity, high-chemoattractant region near the surface of the particle to move into the plume (6)]. A decrease in A_{CHE} (3.8–2.7) with increasing U (66–660 $\mu m\ s^{-1}$) was also observed in numerical simulations of a spherical particle at $\tau_{PHYS} = 300$ s (see *SI Appendix 1*, "Numerical Model").

We tested the relevance of our two-dimensional (2D) findings to 3D plumes in the ocean by numerically comparing nutrient exposure and chemotactic advantage for cylindrical and spherical particles (*SI Appendix 1*, "Numerical Model"). As expected, T_C was smaller in 3D than in 2D (by 6- to 17-fold for $U = 66–660\ \mu m\ s^{-1}$) because concentrations drop more rapidly with distance in 3D and bacteria have an additional dimension to sample. On the other hand, we found A_{CHE} to be comparable between the 2D and 3D scenarios for all values of U and V_B (Fig. 3*d*), suggesting a significant advantage of chemotactic motility also for 3D plumes in the ocean.

Our accumulation data can be used to estimate the fraction of DOM leaking from a particle that is taken up by chemotactic bacteria in the plume. Assuming a scenario with 10^5 bacteria per milliliter, 0.3 μm in radius, and diffusion-limited uptake (19), we calculated that 37% of the DOM released by a particle sinking at $U = 66\ \mu m\ s^{-1}$ would be taken up within the first $y = 20$ mm of its plume ($\tau_{PHYS} = 303$ s). This fraction dropped to 7% and 2% for $U = 220$ and 660 $\mu m\ s^{-1}$. The DOM uptake of chemotactic bacteria relative to nonmotile cells is given by the ratio of T_C for the two populations (A_{CHE}) because both uptake and T_C are linearly proportional to the local instantaneous concentration experienced by bacteria. Over the first 20 mm, uptake by chemotactic bacteria was 187%, 235%, and 270% of that of nonmotile cells for $U = 66$, 220, and 660 $\mu m\ s^{-1}$, respectively (Fig. 3*c*). Numerical simulations revealed that even larger fractions of the plume can be taken up by bacteria in the 3D case, and the comparison of A_{CHE} (Fig. 3*d*) demonstrates that the relative increase in uptake over nonmotile cells is comparable for 2D and 3D plumes, supporting the applicability of our findings to realistic plumes in the ocean.

Discussion

In the ocean, bacteria encounter nutrient patches from a variety of sources (4–8, 10), occurring over a range of time scales (τ_{PHYS}). Some bacteria attach to organic particles or polymeric material (9, 25) or may reside in the nutrient microzone surrounding photosynthesizing phytoplankton cells (4, 7), thus benefiting from persistent nutrient supplies ($\tau_{PHYS} \approx$ hours to days). Here we focused on whether the chemotactic behavior of marine bacteria is appropriate to exploit ephemeral patches ($\tau_{PHYS} \approx$ seconds to minutes), resulting from transient events such as cell lysis, sloppy feeding, or DOM release by sinking particles (2, 5, 25), by using microfluidics to create carefully controlled and environmentally realistic patches.

P. haloplanktis formed intense, submillimeter-scale hot spots within tens of seconds in response to purely diffusive nutrient pulses (Pe = 0) comparable in size to patches arising from predation of phytoplankton cells (2). These hot spots are consistent with previous observations of marine bacteria clustering within oxygen gradients (12, 26) and random lysis events (2) and could contribute to microscale bacterial patchiness detected in

the ocean (27). The short response time allowed *P. haloplanktis* to reach cell concentrations three times above background values well before the patch was eroded by diffusion (i.e., $\tau_{BIO} < \tau_{PHYS}$). This provided up to a 3-fold average advantage in nutrient exposure over a nonmotile population, in line with previous estimates (2). Because patches are typically smaller than the Kolmogorov scale (28), we also expect these conclusions to apply in a turbulent ocean, with occasional high shear rates stretching patches into elongated tendrils rather than dissipating them (5).

This rapid response to nutrient gradients also allows *P. haloplanktis* to exploit DOM plumes (Pe $>$ 0). Colonization of nutrient plumes by marine bacteria has been postulated (6, 9) but never observed, and widespread plume exploitation in the ocean could increase carbon turnover rates (9). Plume colonization depends on particle sinking speed U, which governs the shape of the plume and the time τ_{PHYS} available for bacteria to respond. We observed significant bacterial hot spots in the plume of particles sinking as fast as 220 μm s^{-1}. Taken together with empirical data on sinking speeds of marine snow particles [e.g., U (cm s^{-1}) = 0.2 R (cm) (23)] and fecal pellets (5–30,000 μm s^{-1}) (17), this suggests that marine bacteria could exploit plumes of particles as large as R = 1 mm and of the slower-settling among the fecal pellets, most likely from copepods and euphasiids (17). As we have investigated only the first 24 mm of the plume, faster particles could induce accumulation farther downstream (6), but longer plumes are more likely to be disrupted by turbulence in the ocean (24). The response to the plume resulted in a considerable nutrient exposure advantage over nonmotile cells for all sinking speeds ($A_{CHE} > 2$) and was found to potentially lead to a significant acceleration in turnover rates of particle-released DOM. Because bacterial nutrient exposure is nearly independent of particle size for Pe $>$ 1 (10), these findings may apply to a large proportion of marine snow particles and fecal pellets.

The patchy environment of the ocean poses different survival challenges compared with the nutrient-dense habitat of an enteric bacterium. Indeed, *P. haloplanktis* displayed a markedly shorter response time (τ_{BIO}) than *E. coli*. This resulted in twice the chemotactic advantage A_{CHE} in the first 5 min of a nutrient pulse despite *E. coli* being challenged with two of its most potent chemoattractants, whereas an environmentally realistic, but possibly nonoptimal chemoattractant, was provided to *P. haloplanktis*. The higher speed of *P. haloplanktis* (68 μm s^{-1}) compared with *E. coli* (31 μm s^{-1}) is the most apparent reason for better patch exploitation (6, 29). Considerably faster swimming than *E. coli* has been shown for several marine bacteria (11, 12, 26), which achieve burst speeds up to 445 μm s^{-1} when tracking nutrient sources (30). Modeling confirmed an increase in chemotactic advantage with speed (Fig. 3*a*), yet to a smaller degree than observed in the experiments (Fig. 2*c*), suggesting that *P. haloplanktis* relies on additional behavioral strategies beyond speed to exploit patches. In particular, marine bacteria generally display a "run-and-reverse" swimming strategy where cells almost reverse when turning, rather than the nearly random reorientation of the *E. coli* "run-and-tumble" model (11, 12, 31). Run-and-reverse swimming has been proposed as an adaptive strategy for remaining inside microscale patches (12, 32) and enhancing chemotactic abilities under turbulent conditions (7). At the same time, high-speed chemotactic motility is expensive because the energetic cost of swimming grows quadratically with speed and is heavily taxed by the low (≈1%) efficiency of flagellar motility with significant additional costs from biosynthesis of flagella and regulatory machinery (33). Although our results, together with the widespread occurrence of bacterial motility in the ocean (16, 34), suggest that bacteria derive a substantial benefit from chemotaxis, these costs will have to be accounted for to quantify the competitive advantage of chemotactic motility in different nutrient landscapes.

The proficiency of *P. haloplanktis* in taking advantage of patches and plumes of DOM strongly supports the hypothesis that rapid chemotactic exploitation of microscale resources can accelerate the rates of biogeochemical cycling in the ocean (2, 6), compared with a scenario where bacteria are nonmotile and rely solely on diffusion for DOM uptake. Furthermore, such increases in DOM uptake rates generated by rapid chemotactic clustering may translate to enhanced net biogeochemical fluxes if bacteria can convert a higher fraction of DOM into biomass when exposed to patches and plumes. First, there is considerable evidence that bacterial growth yield increases with growth rate (35) so that bacterial biomass production may be enhanced in patches and plumes compared with the surrounding low-DOM water. Second, because DOM becomes increasingly refractory toward bacterial metabolism (36), rapid uptake of DOM after its release from point sources may increase the net amount of DOM metabolized by bacteria.

It has recently been suggested that ocean bacteria follow at least two different adaptive strategies: the "opportunitroph," actively exploiting patchy resources, and the passive oligotroph, efficiently using low nutrient concentrations (37). Our observations indicate that the response time scale of opportunitrophs can be commensurate with patch evolution time scales, enabling utilization of a wide range of patchily distributed nutrient resources in the ocean. The prevalence of each type may shift depending on the local conditions in the ocean; for example, algal blooms may lead to increased activity of patch specialists. This may explain why current observations on motility in ocean samples are highly variable (16, 34) and indicates that it will be important to quantitatively explore the behavioral response of bacteria to specific nutrient landscapes in the ocean. The results presented here strongly suggest that marine bacteria are capable of responding to ephemeral patches of organic matter before these patches dissipate, indicating that bacterial chemotactic behavior in the ocean may impact planktonic trophodynamics and biogeochemical transformation rates.

Methods

Microfluidics. Microfluidic channels were fabricated by using PDMS and soft lithography, as described previously (38, 39). The microchannel used in the "diffusing nutrient patch" experiments was 45 mm long (with a working section of 25 mm), 3 mm wide, and 50 μm deep, with two in-line inlets to separately introduce bacteria and nutrients (Fig. 1*a*). The nutrient inlet led to a 100-μm-wide PDMS microinjector (Fig. 1*b*), which generated a coherent nutrient band. The microchannel used in the nutrient plume experiments was identical to the first, with the exception of an additional microfabricated PDMS cylinder to simulate a sinking particle. The cylinder had radius R = 250 μm and was centered 290 μm downstream of the tip of the microinjector (Fig. 1*c*).

Bacteria. A culture of *P. haloplanktis* ATCC 700530 was obtained from the American Type Culture Collection and grown overnight to mid-exponential phase in 1% tryptic soy broth at room temperature while agitated on a shaker (175 rpm). Cultures were diluted 1:20 in artificial seawater and starved at room temperature for 72 h (12). *E. coli* HCB1 (provided by H. Berg) was grown in tryptone broth at 34°C on an orbital shaker (220 rpm) to an optical density of 0.4 and then washed thrice by centrifuging at 2,000 × *g* for 5 min, and the pellet was resuspended in Howard Berg motility medium (10 mM potassium phosphate/100 μM EDTA/10 mM NaCl, pH = 7.5).

Attractants. In experiments with *P. haloplanktis*, the chemoattractant consisted of filtrates from cultures of the marine phytoplankton *D. tertiolecta* CCMP1320, by using the techniques of Bell and Mitchell (40). Axenic cultures of *D. tertiolecta* (from the Provasoli–Guillard National Center for Culture of Marine Phytoplankton) were grown in f/2 medium (41) to early exponential phase (1 week, ≈2 × 10^4 cells per milliliter). Culture filtrates were obtained by centrifuging 1-ml aliquots at 900 × *g* for 5 min before filtration through sterile 0.2-μm membrane filters (Millipore). The concentration of DOC in the culture filtrate was obtained by acidifying with phosphoric acid to pH = 2 and bubbling with compressed air to remove inorganic carbon. Nine repeat measurements were taken by using a Shimadzu TOC-5000 total carbon analyzer. The phytoplankton-derived DOC concentration was 6.81 ± 1.37 mg liter^{-1} or

ENVIRONMENTAL SCIENCES

567 ± 114 μM. In experiments with *E. coli*, the chemoattractant was a mixture of 10 μM L-serine and 10 μM L-aspartate (Sigma–Aldrich) in Howard Berg motility medium. In control experiments, 0.2-μm filtrate from the bacterial culture was used in lieu of the chemoattractant. Further control experiments with *P. haloplanktis* were conducted by using f/2 algal culture medium in lieu of the chemoattractant. No significant attraction was observed in any of the control runs.

Experimental Conditions. Chemoattractant and bacteria were simultaneously added to microchannels by means of two separate inlets by using two syringes and a syringe pump (PHD 2000; Harvard Apparatus) and were visualized by using an inverted microscope (TE2000ε; Nikon) with a ×10 objective. The concentration field $C(x,y)$ was obtained from epifluorescence images of 100 μM fluorescein (Fluka) added to nutrients (and controls) before all experiments. Fluorescein (diffusivity $D = 0.5 \times 10^{-9}$ m^2 s^{-1}) is a good proxy for the low molecular weight compounds in DOM and is not a chemoattractant for the bacteria. Bacteria were imaged mid-depth in the channel by using phase contrast microscopy by recording sequences of 5–40 frames (i.e., ''movies'') at 32 fps with a 1,600 × 1,200-pixel (field of view: 0.9 × 1.2 mm) CCD camera (PCO 1600; Cooke). Image analysis software (IPLab; Scanalytics) and Matlab were used to obtain the distribution of bacteria $B(x,y)$. An in-house particle tracking code (BacTrack) was used to reconstruct bacterial trajectories and calculate mean speeds.

In the diffusing nutrient patch experiments, bacteria and nutrients were introduced into the channel at 220 μm s^{-1}. After the flow was stopped (time $t = 0$), across-channel distributions $C(x)$ and $B(x)$ were measured every 13 s for at least 13 min. At each point in time, a mosaic of three images was obtained by computer-controlled motion of the microscope stage to cover the entire channel width. $C(x)$ was obtained by averaging $C(x,y)$ in the downstream direction y over the field of view. At least 2,400 bacteria were counted for each time point. In the nutrient plume experiments, bacteria and nutrients were injected at a constant flow rate. $B(x,y)$ and $C(x,y)$ were measured every $\Delta y = 1.5$ mm, to a distance of 20–24 mm downstream of the particle. At each position y, three across-channel images were obtained, as above. At least 10^5 bacteria were counted in each plume. To calculate the chemotactic advantage A_{CHE}, experiments were repeated with 2-μm beads as a proxy for nonmotile bacteria. Experiments to determine the mean swimming speed V_B of *P. haloplanktis* and *E. coli* were conducted in microchannels without nutrients or flow.

Numerical Model. The model is described in *SI Appendix 1*.

ACKNOWLEDGMENTS. We thank P. Chisholm and G. Jackson for comments on an initial version of this manuscript; H. Berg and L. Turner for providing *E. coli* and advice on chemoattractants; T. Ahmed and Marcos for help with microfabrication; W. Durham and L. Fernandez for help with DOC measurements; S. Stransky for developing BacTrack; H. Ducklow, J. Hobbie, D. Repeta, and D. McGillicuddy for useful discussions; and two anonymous reviewers for insightful comments. R.S. thanks A. van Oudenaarden for hospitality in his laboratory at the onset of this project. This work was supported by National Science Foundation Grant OCE-0526241 (to R.S. and M.F.P.) and grants by the Department of Energy Genomes to Life program, the National Science Foundation/National Institute on Environmental Health Sciences cosponsored Woods Hole Center for Ocean and Human Health, and the Gordon and Betty Moore Foundation (to M.F.P.).

1. Azam F (1998) Microbial control of oceanic carbon flux: The plot thickens. *Science* 280:694–696.
2. Blackburn N, Fenchel T, Mitchell J (1998) Microscale nutrient patches in planktonic habitats shown by chemotactic bacteria. *Science* 282:2254–2256.
3. Fenchel T (2002) Microbial behavior in a heterogeneous world. *Science* 296:1068–1071.
4. Mitchell JG, Okubo A, Fuhrman JA (1985) Microzones surrounding phytoplankton form the basis for a stratified marine microbial ecosystem. *Nature* 316:58–59.
5. Blackburn N, Azam F, Hågström A (1997) Spatially explicit simulations of a microbial food web. *Limnol Oceanogr* 42:613–622.
6. Kiørboe T, Jackson GA (2001) Marine snow, organic solute plumes, and optimal chemosensory behavior of bacteria. *Limnol Oceanogr* 46:1309–1318.
7. Bowen JD, Stolzenbach KD, Chisholm SW (1993) Simulating bacterial clustering around phytoplankton cells in a turbulent ocean. *Limnol Oceanogr* 38:36–51.
8. Lehman JT, Scavia D (1982) Microscale patchiness of nutrients in plankton communities. *Science* 216:729.
9. Azam F, Long RA (2001) Oceanography–Sea snow microcosms. *Nature* 414:495–498.
10. Jackson GA (1989) Simulation of bacterial attraction and adhesion to falling particles in an aquatic environment. *Limnol Oceanogr* 34:514–530.
11. Barbara GM, Mitchell JG (2003) Marine bacterial organisation around point-like sources of amino acids. *FEMS Microbiol Ecol* 43:99–109.
12. Mitchell JG, Pearson L, Dillon S (1996) Clustering of marine bacteria in seawater enrichments. *Appl Environ Microbiol* 62:3716–3721.
13. Mao HB, Cremer PS, Manson MD (2003) A sensitive, versatile microfluidic assay for bacterial chemotaxis. *Proc Natl Acad Sci USA* 100:5449–5454.
14. Keymer JE *et al.* (2006) Bacterial metapopulations in nanofabricated landscapes. *Proc Natl Acad Sci USA* 103:17290.
15. Park S *et al.* (2003) Motion to form a quorum. *Science* 301:188.
16. Grossart HP, Riemann L, Azam F (2001) Bacterial motility in the sea and its ecological implications. *Aquat Microb Ecol* 25:247–258.
17. Turner JT (2002) Zooplankton fecal pellets, marine snow and sinking phytoplankton blooms. *Aquat Microb Ecol* 27:57–102.
18. Gobler CJ, Boneillo GE, Debenham CJ, Caron DA (2004) Nutrient limitation, organic matter cycling, and plankton dynamics during an Aureococcus anophagefferens bloom. *Aquat Microb Ecol* 35:31–43.
19. Berg HC (1983) *Random Walks in Biology* (Princeton University Press, Princeton, NJ).
20. Urban–Rich J (1999) Release of dissolved organic carbon from copepod fecal pellets in the Greenland Sea. *J Exp Mar Biol Ecol* 232:107–124.
21. Smith DC, Simon M, Alldredge AL, Azam F (1992) Intense hydrolytic enzyme activity on marine aggregates and implications for rapid particle dissolution. *Nature* 359:139–142.
22. Alldredge AL, Gotschalk C (1988) In situ settling behavior of marine snow. *Limnol Oceanogr* 33:339–351.
23. Alldredge AL, Gotschalk CC (1989) Direct observations of the mass flocculation of diatom blooms: Characteristics, settling velocities and formation of diatom aggregates. *Deep-Sea Res* 36:159–171.
24. Visser AW, Jackson GA (2004) Characteristics of the chemical plume behind a sinking particle in a turbulent water column. *Mar Ecol Prog Ser* 283:55–71.
25. Kiørboe T, Grossart HP, Ploug H, Tang K (2002) Mechanisms and rates of bacterial colonization of sinking aggregates. *Appl Environ Microbiol* 68:3996–4006.
26. Mitchell JG *et al.* (1995) Long lag times and high velocities in the motility of natural assemblages of marine bacteria. *Appl Environ Microbiol* 61:877–882.
27. Seymour JR, Mitchell JG, Seuront L (2004) Microscale heterogeneity in the activity of coastal bacterioplankton communities. *Aquat Microb Ecol* 35:1–16.
28. Lazier JRN, Mann KH (1989) Turbulence and the diffusive layers around small organisms. *Deep-Sea Res* 36:1721–1733.
29. Blackburn N, Fenchel T (1999) Influence of bacteria, diffusion and sheer on micro-scale nutrient patches, and implications for bacterial chemotaxis. *Mar Ecol Prog Ser* 189:1–7.
30. Barbara GM, Mitchell JG (2003) Bacterial tracking of motile algae. *FEMS Microbiol Ecol* 44:79–87.
31. Johansen JE *et al.* (2002) Variability in motility characteristics among marine bacteria. *Aquat Microb Ecol* 28:229–237.
32. Luchsinger RH, Bergersen B, Mitchell JG (1999) Bacterial swimming strategies and turbulence. *Biophys J* 77:2377–2386.
33. Mitchell JG (2002) The energetics and scaling of search strategies in bacteria. *Am Nat* 160:727–740.
34. Fenchel T (2001) Eppur si muove: Many water column bacteria are motile. *Aquat Microb Ecol* 24:197–201.
35. del Giorgio PA, Cole JJ (1998) Bacterial growth efficiency in natural aquatic systems. *Ann Rev Ecol Syst* 29:503–541.
36. Keil RG, Kirchman DL (1994) Abiotic transformation of labile protein to refractory protein in sea water. *Mar Chem* 45:187–196.
37. Polz MF, Hunt DE, Preheim SP, Weinreich DM (2006) Patterns and mechanisms of genetic and phenotypic differentiation in marine microbes. *Philos Trans R Soc London Ser B* 361:2009–2021.
38. Marcos, Stocker R (2006) Microorganisms in vortices: A microfluidic setup. *Limnol Oceanogr Meth* 4:392–398.
39. Whitesides GM, *et al.* (2001) Soft lithography in biology and biochemistry. *Ann Rev Biomed Eng* 3:335–373.
40. Bell W, Mitchell R (1972) Chemotactic and growth responses of marine bacteria to algal extracellular products. *Biol Bull (Woods Hole, Mass)* 143:265.
41. Guillard RRL, Ryther JH (1962) Studies of marine plankton dynamics. *Can J Microbiol* 8:229–239.